Multifunctional Materials: Transparent Reactive Armor Utilizing Single-Walled Carbon Nanotube Frameworks

Prof. Michael S. Strano, MIT, Chemical Engineering

The goal of this project is to enable a new class of transparent energetic materials from nanotube-organic scaffolds, evaluate the feasibility of transparent reactive armor for defense applications, and to characterize and develop design rules for such materials through preliminary measurements of their properties. Specifically, we focused on developing thin one-dimensional (1-D) chemical actuators with high velocity and high thrust-to-mass ratio. We have completed extensive modeling and the development of engineering design rules. We synthesized and demonstrated the feasibility of several new types of nano-energetic materials.

1. Concept: Transparent Reactive Armor

Explosive Reactive Armor[1-4] (ERA) is a currently deployed means of effectively reducing the penetration ability of kinetic energy (KE) and chemical energy (CE) projectiles through conventional armor (Fig 1a). Briefly, an explosion between two parallel steel plates forces the outer into the path of the incoming projectile with two effects: the penetration distance experienced by the projectile is increased, and some initial momentum[5] is lost to the oppositely traveling plate. Current polycarbonate-based bullet resistant glass technology is limited in several respects: its ability to defeat high velocity
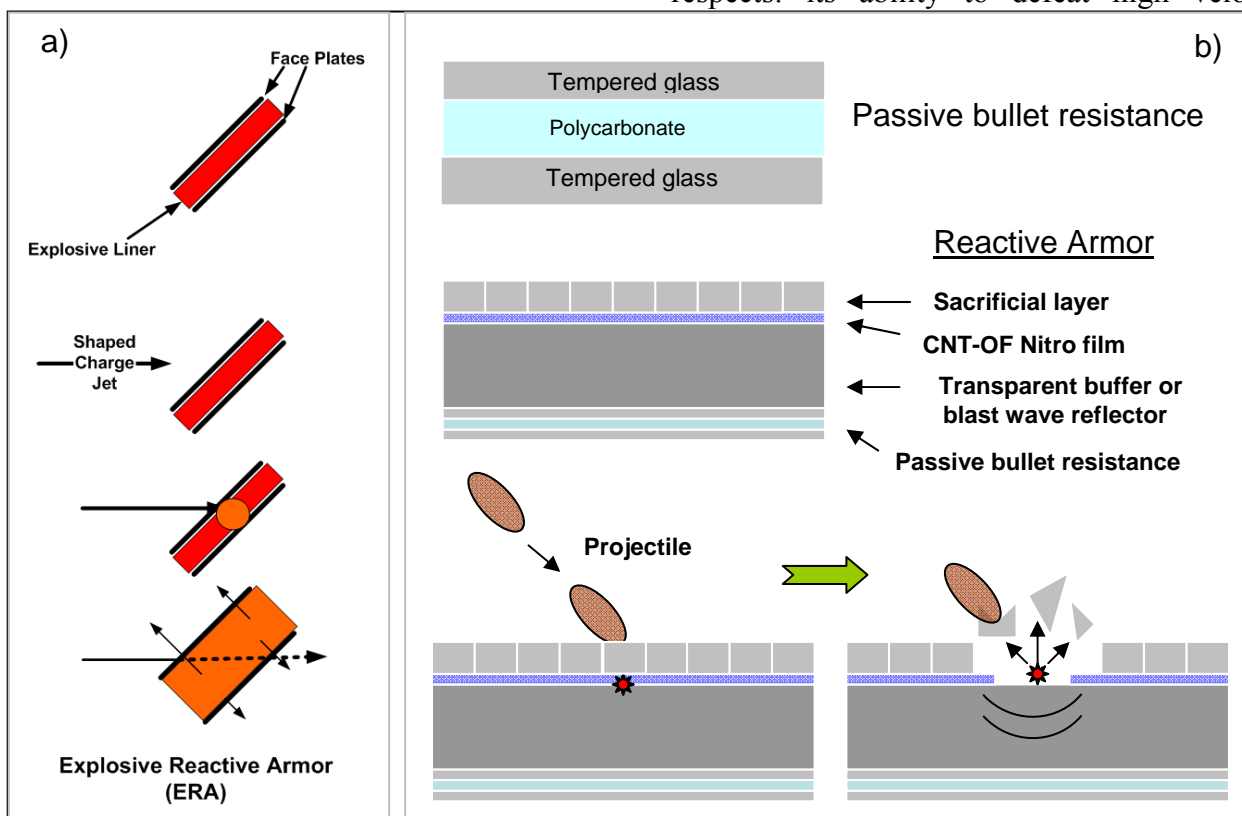

Figure 1: The objective of this project is to create a new class of transparent energetic materials from nanotube-organic scaffolds, evaluate the feasibility of transparent reactive armor for defense applications, characterize and develop design rules for such materials through preliminary measurements of their properties. a) Reactive armor utilizes chemical energy to separate two plates at the moment of penetration by a projectile. The projectile experiences a longer path length through the material and transfer of momentum from the plate. b) Final goal: new materials to extend this concept to transparent materials.

Report Documentation Page

Public reporting burden for the collection of information is estimated to average 1 hour per response, including the time for reviewing instructions, searching existing data sources, gathering and maintaining the data needed, and completing and reviewing the collection of information. Send comments regarding this burden estimate or any other aspect of this collection of information, including suggestions for reducing this burden, to Washington Headquarters Services, Directorate for Information Operations and Reports, 1215 Jefferson Davis Highway, Suite 1204, Arlington VA 22202-4302. Respondents should be aware that notwithstanding any other provision of law, no person shall be subject to a penalty for failing to comply with a collection of information if it does not display a currently valid OMB control number.

1. REPORT DATE **02 MAR 2010**	2. REPORT TYPE	3. DATES COVERED

4. TITLE AND SUBTITLE **Transparent Reactive Armor from SWCNT Organic Frameworks**	5a. CONTRACT NUMBER
	5b. GRANT NUMBER
	5c. PROGRAM ELEMENT NUMBER
6. AUTHOR(S) **Michael Strano**	5d. PROJECT NUMBER
	5e. TASK NUMBER
	5f. WORK UNIT NUMBER

7. PERFORMING ORGANIZATION NAME(S) AND ADDRESS(ES) **Department of Chemical Engineering,Massachusetts Institute of Technology,Cambridge ,MA,02139**	8. PERFORMING ORGANIZATION REPORT NUMBER

9. SPONSORING/MONITORING AGENCY NAME(S) AND ADDRESS(ES)	10. SPONSOR/MONITOR'S ACRONYM(S)
	11. SPONSOR/MONITOR'S REPORT NUMBER(S)

12. DISTRIBUTION/AVAILABILITY STATEMENT
Approved for public release; distribution unlimited.

13. SUPPLEMENTARY NOTES

14. ABSTRACT

The goal of this project is to enable a new class of transparent energetic materials from nanotube-organic scaffolds, evaluate the feasibility of transparent reactive armor for defense applications, and to characterize and develop design rules for such materials through preliminary measurements of their properties. Specifically, we focused on developing thin one-dimensional (1-D) chemical actuators with high velocity and high thrust-to-mass ratio. We have completed extensive modeling and the development of engineering design rules. We synthesized and demonstrated the feasibility of several new types of nano-energetic materials.

15. SUBJECT TERMS

16. SECURITY CLASSIFICATION OF:			17. LIMITATION OF ABSTRACT	18. NUMBER OF PAGES **12**	19a. NAME OF RESPONSIBLE PERSON
a. REPORT **unclassified**	b. ABSTRACT **unclassified**	c. THIS PAGE **unclassified**			

kinetic energy rounds and explosive (CE) projectiles[6] because of the transparency requirement. Also the mass of the armor must increase to meet a certain level of resistance. Reactive armor for transparent materials could lead to a paradigm shift in ballistic defense: the use of chemical energy to defeat a projectile instead of passive dissipation of the energy. It may find widespread usage in weight sensitive applications or highly-damaging environments.

A hypothetical design would employ a sacrificial ply on top of an energetic transparent film (Fig 1b). This film resides on a backing designed to resist or buffer the surface blast from damaging the underlying transparent support. Innovative engineering designs can be used to direct a portion of the energy towards the projectile, such as shape-charge geometries and wave-guides for the released energy. Such a design could, in theory, significantly extend the defense of passive bullet resistance to systems with dramatically lower weight. Several technological innovations are necessary to experimentally evaluate this goal: the film must be robust, transparent and energetic with chemically and structurally tunable impulse pressure. This film must form composite laminates with other transparent materials, and demonstrate suitable transfer of stored chemical energy to mechanical actuation of the sacrificial ply.

2. *Theoretical Understanding of Chemical Energy Propagation along a 1D Conduit – Nanothermites*

Our first theoretical investigation examined 1-D nanothermites as the simplest test case. The concept is to use a single-walled carbon nanotube (SWNT) as a thermal conduit to accelerate the oxidation of an annular Al or
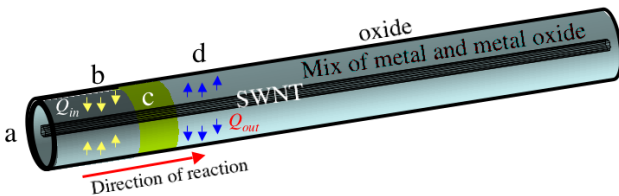
Figure 2. Conceptual design of an anisotropic nanothermite based upon a metal nanoparticle-SWNT model system.

Zr shell (Figure 2).[7] We numerically solved the coupled energy balances for a carbon nanotube with an annular coating of reactive metal, such that coupling to thermal transport in the nanotube accelerates reaction in the annulus.
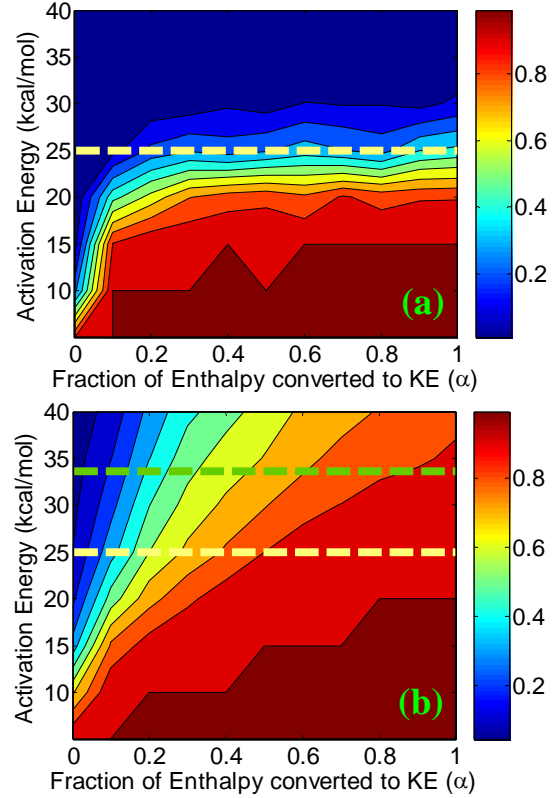
Figure 3. Stability plots for 2 EM/bead. (a) The system was equilibrated at 300 K and allowed to evolve in time without initial excitation. Average conversions have been plotted as a function of E_a and α. (b) Same system but with excitation at $t = 0$.

For the case of Zr metal, the nanotube increases the velocity of the reaction front in the direction of the nanotube length from 530 to 5100 mm/s. Nanotube conductivity as well as the relative sizes of the Zr annulus and the nanotube limit enhancement of the reaction velocity to a maximum of a factor of ~10. Interestingly, the interfacial heat conductance is not the most significant factor affecting the coupling, due to the large temperature differences (more than 1000 K) between nanotube and annulus at the reaction front and directional heat conduction in the nanotube. This work demonstrates that the principle – directed energy release – is possible; it was published in the journal *Nanotechnology*.[7]

3. A Stochastic Molecular Dynamics Model of 1D Energetic Lattice Materials

In the model, a nanotube is loaded with trinitrophenylbenzene groups at regular intervals. A shock applied at one end leads to the decomposition of the group. The 1-D nature of the nanotube can be used to channel the energy released during reaction. We seek to identify conditions under which sustained chain reactions are feasible. The following system parameters are varied: (a) activation energy of the reaction, E_a; (b) fraction of the reaction enthalpy that is converted into the kinetic energy (KE) of the reacted fragments, α. Zones of stability of the nanostructure as well as the velocity of the reaction wave can be mapped out. The effect of loading of the EM has also been studied for pristine and defect-laden nanotubes.

3.1 Model Development

3.1.1 Force Balance

The force-field and the associated parameters have already been specified in the literature.[8] In the coarse-grained model, the total force on the ith bead of mass m_i in terms of the tensile ($F_{s,i}$), bending ($F_{b,i}$) and non-bonding ($F_{nb,i}$) components is:

$$m_i a_i = F_{s,i} + F_{b,i} + F_{nb,i} \qquad (1)$$

where a_i is the acceleration of the bead.

3.1.2 Energy Conversion

The chemical energy released during the reaction (ΔH) is deposited in the kinetic component of the local bead. The fraction, α, determines the amount of enthalpy that is converted to the KE of the reaction products. Equating the total energy of the system and surroundings before and after a reaction at a certain location in the chain gives

$$2\alpha\Delta H = m_b v_b^2 + m_e v_e^2 - \left(m_b + m_e\right)u^2 \quad (2)$$

In the above equation, the reaction fragments are the pristine bead and the decomposition products of the EM. The first two terms represent the final kinetic energies of these species. We only consider the center of mass (CM) of the latter set in the analysis to simplify matters. It follows that m_e (v_e) is the mass (velocity) of the CM of the reaction products of the molecule. The last term denotes the initial KE of the unreacted bead, where u is the velocity of the bead prior to the reaction.

In a given time step, all the quantities in eq. 2 except for the final velocities – v_b and v_e – are known. The conservation of momentum gives us a second relationship between the product velocities

$$\left(m_b + m_e\right)\vec{u} = m_b \vec{v}_b + m_e \vec{v}_e \qquad (3)$$

which in conjunction with eq. 2 can be used to solve for the unknowns.

3.2 Parametric Study of Reactions

The number of beads in the chain was fixed at 100. The mass of each bead is 1953 amu, and is equivalent to 163 carbon atoms. We perform the analysis for a load of 2 EM/bead. On a finer basis, the loading is 2 EM per 81 carbon atoms. The heat of explosion of TNT (2732.48 kJ/kg)[9] was used as a representative value for ΔH in the simulation. The lattice was initially equilibrated at 300 K and was allowed to evolve in time over a period covering ~7 ps.

The first step was to ascertain the stability of the nanomaterial as a function of the activation energy of the EM (E_a) and α. After equilibration, the system was allowed to evolve in time and reaction events were recorded. The average conversion has been plotted in Figure 3a for 2 EM/bead as a function of the 2 parameters. It is observed that 80% of the EM present on the SWNTS react without an external stimulus for $E_a < 25$ kcal/mol; at low activation barriers, the reaction sites are energetic enough to obviate the need for a prior excitation. This test establishes a lower limit for the selection of molecules in the design of such structures.

The effect of an excitation at time $t = 0$ was studied by cleaving the bead-EM link at the first node unconditionally and tracking the progress of the reaction wave with time. Figure 3b shows the conversion plot for 2 EM/bead along with the stability limits obtained from Figure 3a and the activation energy for the thermal decomposition of TNT (~33 kcal/mol)[10] as a reference point. For loads of 1 molecule/bead or less, negligible difference is expected between cases of finite and zero initial excitation. This is understandable, since the
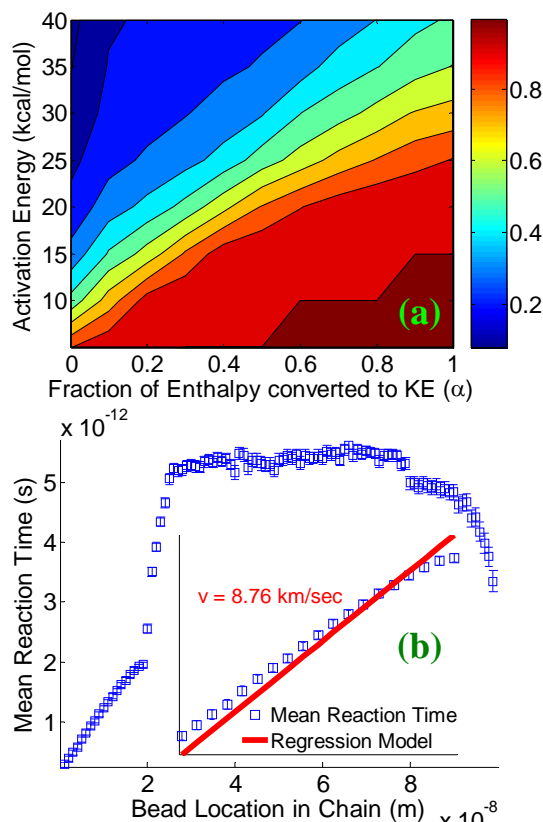
3

Figure 4. (a) Conversion and (b) velocity plots (2 EM/bead) with the introduction of 4 defects along the length of the chain.

defective SWNT under similar circumstances. In addition, the velocity plot in Figures 4b indicates that the very first defect in the lattice disrupts the linear progression of reactions, after which the pattern is more random. This could possibly be due to the localization of energy at the defects. The disturbance is communicated to the subsequent beads at a much slower pace and causes them to react in a haphazard fashion albeit after a longer time interval.

The velocity of the reaction wave computed from the linear sections ($\alpha = 0.7$) is similar to the pristine case (~8.8 km/sec), which makes sense due to the absence of defects in this portion of the nanotube.

Scheme 1: Synthesis of nitrophenyl functionalized SWNTs (MNP-, DNP-, and TNP-SWNT) utilizing diazonium chemistry.

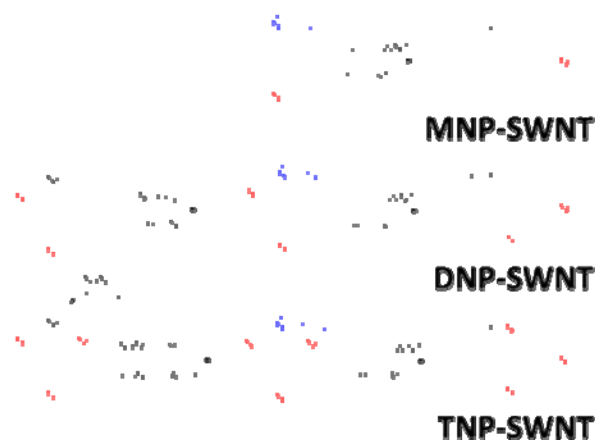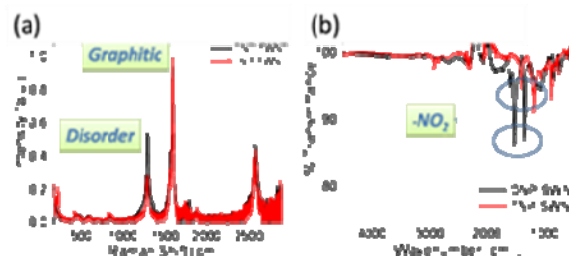sparse EM coverage leads to little or no momentum transfer to the bead in the event a reaction occurs.

A reaction wave velocity of 9.18 km/s has been computed for $\alpha = 0.7$. The speed of sound in carbon nanotubes has been theoretically found to be 14 km/s and 21 km/s for the torsional and longitudinal modes, respectively.[11]

3.3 Effect of Defects

Defects were introduced in the chain of oscillators by lowering the tensile and bending force constants by a factor of 50 at 190, 390, 590 and 790 Å (Figure 3a,b). The simulations were run for the 2 EM/bead case and can therefore be compared to Figures 3b and 4. The contour plots in Figure 4a shows a distinct reduction in reactivities with the presence of defects in comparison to the pristine SWNT in Figure 3b. It is interesting to note the average conversion at $E_a = 35$ kcal/mol is around 50% even at $\alpha = 1$, whereas it was ~1 for the non-

Figure 5: Raman spectroscopy (a, excited at 785 nm) and FT-IR (b, ATR accessory) for films of DNP- (black) and TNP-SWNT (red).
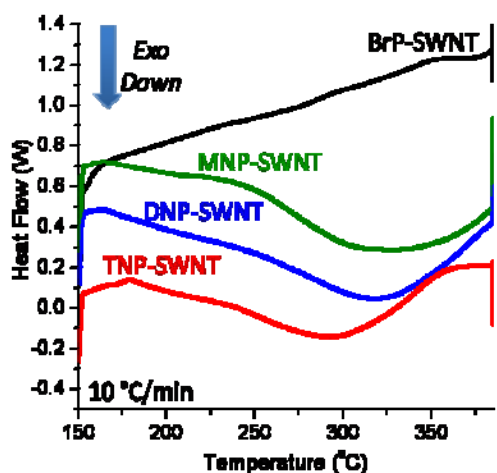
Figure 6. DSC heat flow (exothermic down) with temperature scanning (10 °C/min) under nitrogen for BrPh-SWNT (black), MNP-SWNT (green), DNP-SWNT (blue), and TNP-SWNT (red).

4. Synthesis of Nitrophenyl Carbon Nanotubes

Energetically decorated SWNTs were successfully synthesized with polynitrophenyl groups utilizing diazonium chemistry.[12] As described in Scheme 1, mono- (M-), di- (D-), and trinitrophenyl (TNP) diazonium salts were prepared from corresponding anilines,[13] and subjected to a functionalization reaction with surfactant- (sodium dodecyl sulfate a.k.a. SDS) dispersed SWNT solution.[14] The stability of diazonium salts in the mixture is inversely proportional to the number of attached functional groups (mono < di < tri). Thus, more concentrated reagent was needed for DNP-SWNT than for MNP-SWNT if a similar level of functionalization was desired. However, for TNP-SWNT, a certain level of functionalization or more was not achieved before the SWNTs flocculated, mainly due to the significant instability of TNP-N_2^+ salt and low solubility of the product. Repeated reaction with re-dispersed SWNTs increased the level of functionalization slightly.

Raman and FTIR spectroscopy (Figure 5) verified functionalization of nitrophenyl groups. As expected, the covalent attachment of functional groups increased the disorder mode (D-peak, ~1300 cm^{-1}) in Raman excited at 785 nm. Samples with various D/G ratios were produced when starting with different concentrations of diazonium salts. FTIR (with ATR accessory) clearly showed the existence of nitro groups in the samples (Figure 5b).

The energy release properties of these functionalized SWNTs were demonstrated in differential scanning calorimetry (DSC) (Figure 6).[10,15-16] Samples with masses of 0.3~0.6 mg, and the temperature was scanned from 150 to 385 °C at 10 °C/min under nitrogen. For comparison, SWNTs functionalized with a non-energetic group (4-bromophenyl) exhibited almost no heat generation.

Remarkably, energetically decorated SWNTs generated considerable heat when decomposing at high temperatures. The heat released depends on the total number of nitro groups, which in turn depends on the type of moiety and the number of attached groups. It should be noted that MNP-SWNT has the highest level of functionalization and TNP-SWNT has the lowest, which is the reason why all NP-SWNTs appear to produce similar amount of heat.

The reaction completed within the scanning cycle for TNP-SWNT but not for DNP- and MNP-SWNT. In addition, the conversions at the same temperature were in the order of TNP-, DNP-, and MNP-SWNT. We believe this is due to the differences in activation energies for decomposition and thus TNP-SWNT has the lowest activation energy. Considering the significant amount of heat release and the low activation energy, NP-SWNTs, especially TNP-SWNTs, are highly promising nanoenergetic materials for sustainable 1-D reaction propagation, directional energy release.
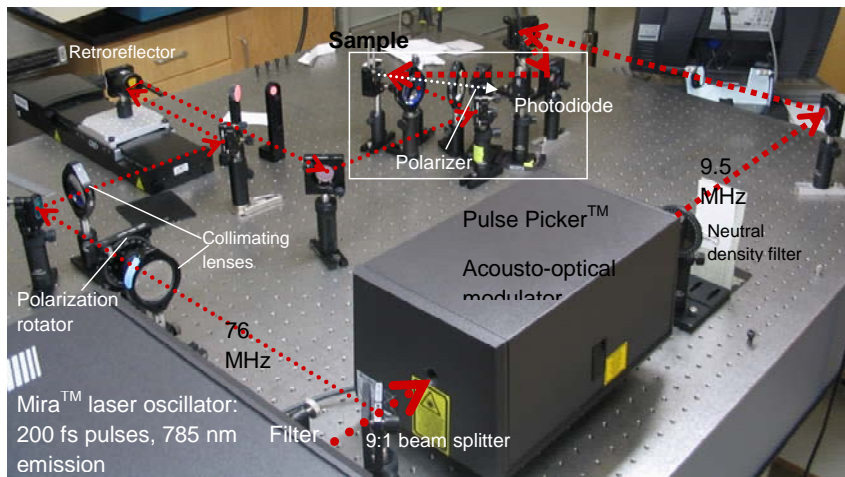
5

Figure 7: TTR setup in the Strano lab.

5. Transient Thermoreflectance for Quantifying Phonon Transport in Nanostructures

Researchers have used transient thermoreflectance (TTR) and the closely related technique of transient thermotransmittance (TTT) to study heat transfer at very small scales for more than twenty years.[17-19] So far, the need to manage heat in microelectronics has motivated studies of thin films of semiconductors[18,20-24] and metals,[17,19,24-26] as well as the interface between the two.[20,22,27-28] However, we have seen an opportunity to apply these techniques to novel thermal measurements of nanostructures and individual molecules. For example, only a few studies have been published addressing the anisotropic nature of heat transport in SWNTs.[29-31]

In metal films with thickness on the order of 100 nm, it takes about 100 ps after heating for the substrate to affect surface temperature.[24] A femtosecond pulsed laser can heat a sample almost instantaneously relative to this time scale. One can split the pulsed laser beam into a higher-energy pump beam to heat a sample and a lower-energy probe beam, as shown in the setup in Figure 7, to track the sample's reflectivity. Reflectivity is a function of the dielectric constant of a material, which depends on temperature and strain,[24] so we can use TTR to create a temperature profile. From there we can calculate parameters like thermal conductivity[19,22-25] and interfacial resistance.[20,22,27-28]

6. Testing towards Self-Actuating Reactive Armor Composites

6.1 Film fabrication

Transparent SWNT films were synthesized by a previously reported filtration method. Transparency can be controlled by the thickness of the film. The film was transferred to a flexible PDMS membrane for electrical detection of rapid mechanical loading. When a projectile traveling ~100 m/s impacts the film, the resulting transient deformation creates a measurable change in film impedance. This resistance change arises from several sources. At low deformation, matrix strain changes the number of percolating conduction pathways in the film. For larger deformations, lattice strain can alter the SWNT band gap. In these preliminary experiments, the response speed was rapid (under 100 μs). Because the SWNT film has a low capacitance and sensitive electro-mechanical properties, it can actuate the proposed reactive armor scheme. The ability to transduce rapid loading on the microsecond time scale allows for initiation of the energetic reaction in response to ballistic penetration (Figure 8).
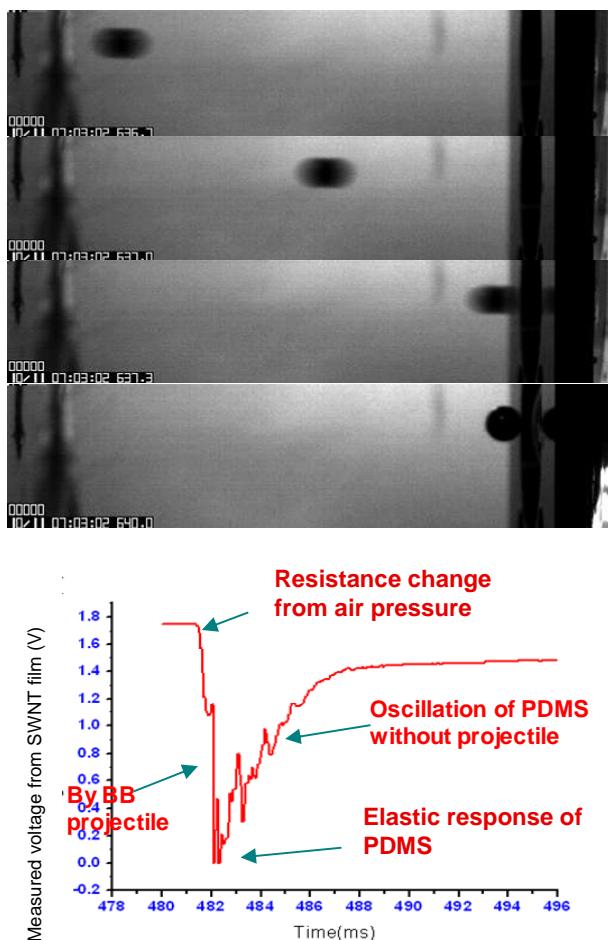
Figure 8: (top) High speed camera images of a projectile impinging on a SWNT/PDMS composite. (bottom) Voltage trace of the rapid loading and subsequent oscillations as electrically transduced by the SWNT.

6.2 1-D propulsion of vertically aligned SWNT film mixed with RDX and sodium azide

Vertically aligned SWNTs were grown by a CVD method previously reported. These arrays have high packing densities but contain some void space. A mixture of energetic materials (RDX and sodium azide) were deposited within the porosity of the vertical film and initiated by high voltage electrical discharge between copper electrodes. Control experiments resulted in no reaction. We speculate that the rapid reaction of the film was due to the high thermal conductivity of SWNTs and high packing density of the RDX and sodium azide within the film's pores. This system is a promising candidate for 1-D reactive armor applications.

6.3 Detonation of energetic materials between flexible membranes

We constructed a setup to test the ability of our thin film laminates to actuate rapidly due to energetic release. The mixture described above was placed between flexible PDMS membranes to demonstrate the reactive armor concept on a model ballistic projectile. In this setup, a thin film of RDX/sodium azide mixture was placed between two PDMS membranes. A high voltage electrical discharge initiated reaction. We observed the membrane deformation to an elliptical form that persisted for a period of the reaction and then relaxed to its previous shape. This experimental setup is the initial step to testing future reactive armor candidates.

7. Controllable Synthesis of SWNT Framework Materials

The controlled assembly of nanoparticles is challenging but may potentially create new classes of materials with unique combinations of properties.[32-33] we have been interested in assembling single-walled carbon nanotubes (SWNTs) into three-dimensional (3-D) framework structures. Toward such aims, SWNT framework multilayers with different linker molecules were synthesized by covalent attachment and subsequently characterized. The flux ratio comparison in a membrane-permeation experiment showed that SWNT framework membranes using larger linker molecules showed larger pore structures. This synthetic method was equally efficient on silica microspheres, resulting in all-SWNT hollow capsules after etching to remove the silica. We were able to further extend the technique to encapsulating gold nanoparticles with perm-selective SWNT cages, potentially a "cell-like" synthetic reaction system.

The SWNT assembly started with diazonium-assisted functionalization[12,34] of 4-carboxyphenyl groups on the SWNT surface,[35] which enabled covalent linkage with diamines
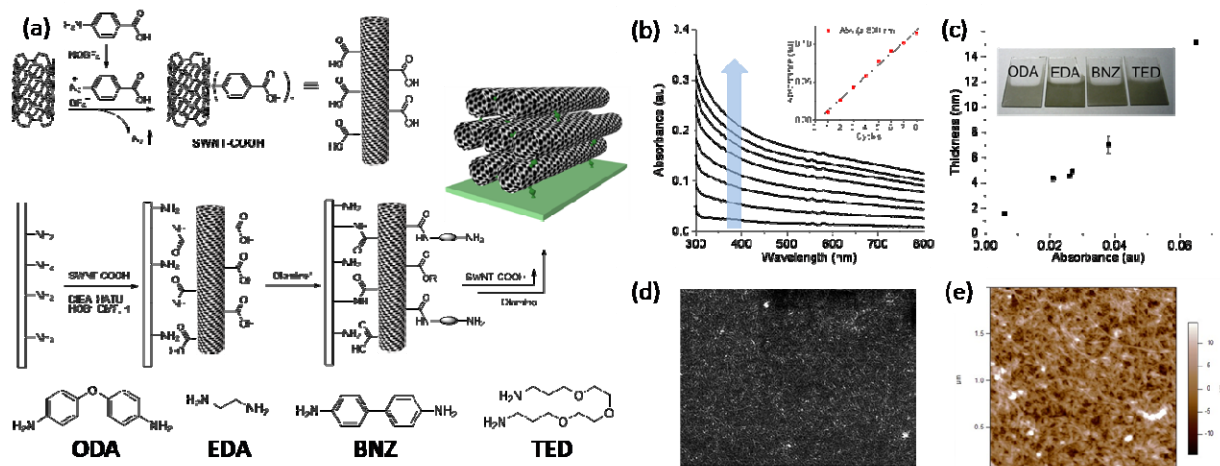
7

Figure 9. Synthesis of SWNT-based framework materials with various amine linkers via amidation chemistry (a), and characterizations of SWNT framework films by UV-visual spectroscopy (b), spectroscopic ellipsometry (c), SEM (d), and AFM (e).

through amidation (Figure 9a). The presence of carboxyl groups was also detected by FT-IR spectroscopy (~1720 cm^{-1}). The carboxyphenyl SWNTs (CxP-SWNTs) were purified and re-dispersed in DMF for the next steps.

Amine-functionalized glass slides were immersed in the DMF solution of CxP-SWNTs for 30 min in the presence of diisopropylethylamine (DIEA, 5 mM), 2-(1H-7-azabenzotriazol-1-yl)-1,1,3,3-tetramethyluronium hexafluorophosphate (HATU, 1 mM), and *N*-hydroxybenzotriazol (HOBt, 2 mM). After being washed with DMF, the glass slides were quickly immersed in the DMF solution of a particular diamine linker (5 mM) for an additional 30 min. This deposition concluded one cycle and cycles were repeated until desired SWNT framework films were obtained.

The selected diamine linker molecules range from short ethylenediamine (EDA) to longer and rigid 4,4'-diaminobiphenyl (benzidine, BNZ) and 4-oxydianiline (ODA), to long but flexible 4,7,10-trioxa-1,13-tridecanediamine (TED), whose maximum end-to-end distances would be 1.7, 2.3, 2.3, and 3.0 nm, respectively, when fully stretched including carboxyphenyl moieties.[36] However, it is likely that the molecules' rigidity or flexibility would greatly affect the actual inter-tube distances.

The build-up of SWNT framework layers was monitored by UV-visual spectrometry (Figure 9b). A broad absorption in the UV and visible ranges from CxP-SWNTs gradually increased as the cycle repeated. The thickness measurements by spectroscopic ellipsometry revealed the linear relationship between the thickness and UV-vis absorbance (Figure 9). It appears that after each cycle, the thickness of SWNT films increases by 3 – 4 nm on average, which is equal to or slightly larger than the thickness of a monolayer of SWNTs and the diamine spacers.

We observed an interconnected network structure of individual SWNTs in scanning electron microscopy (SEM) and AFM (Figure 9d and e, respectively). They are randomly oriented but relatively uniform with apparently reduced bundling of SWNTs. Although SWNTs are not aligned with each other in the assembly, the majority of SWNTs appear to be separated individually, capable of maximizing the functional surface area in the framework structure and potentially controlling the pore sizes.

We performed nanoindentation measurements using AFM, and we were able to confirm that the spring constant of the SWNT framework film increases to 22.6 ± 1.2 N/m (n = 26, sampling number) from the control value 10.4 ± 0.1 N/m (n = 31). Although more control experiments need to be performed, this preliminary result highlights the advantage of
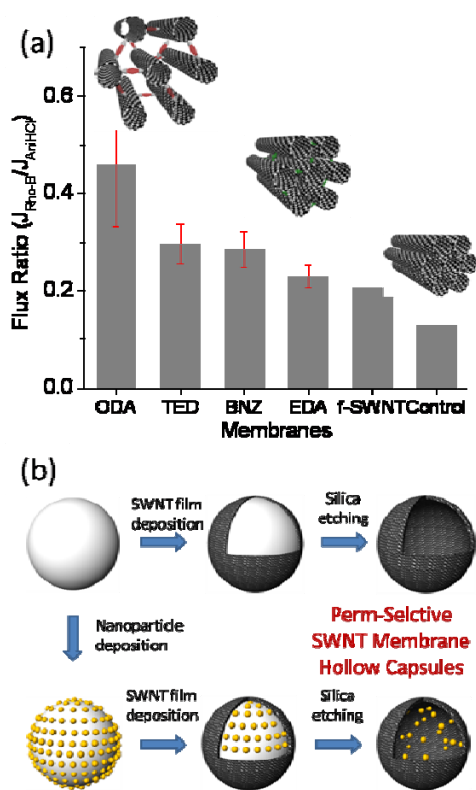
Figure 10. (a) Flux ratio plot from membrane-permeation experiments with Rhodamine B and aniline hydrochloride. (b) Schematic representation of the syntheses of an all-SWNT capsule and its encapsulation of gold nanoparticles.

our covalent method, especially for ultra-thin membrane fabrications.

Pore size differences in the SWNT framework films have been demonstrated by a simple membrane-permeation experiment.[37] SWNT framework films were deposited onto porous anodized alumina discs (pore size 0.2 μm) with 10 cycles (~35 nm), and the films were mounted on the bottom of the inner chamber. We measured the trans-membrane diffusion rates of solute molecules of different sizes, aniline hydrochloride (AniHCl) and Rhodamine B (Rho-B), and their flux ratios were compared.

The obtained flux ratios are plotted in Figure 10a. It should be noted that the larger flux ratio corresponds to a smaller restrictive force and thus a larger pore diameter. From the results, we found that SWNT framework membranes generally exhibit a larger pore structure than the "control" SWNT membrane

(pristine buckypaper). It is likely that SWNTs in the control membrane aggregate into bundles, resulting in a relatively compact structure. Furthermore, the pores from the functionalized, but not cross-linked, SWNT (f-SWNT) membranes appear to be even smaller than those from the SWNT framework membranes, which illustrates that diamine linkages can create and control membrane pore sizes.

The pore diameters of SWNT framework membranes roughly correlate with the lengths of diamine linkers. The large linker, ODA, (inter-tube distance = 2.3 nm) yielded a larger pore SWNT framework membrane than EDA (1.7 nm). The very long but flexible linker, TED, created a membrane with intermediately sized pores. However, the most rigid linker, BNZ, also produced an intermediately sized-pore membrane. The membrane-permeation experiments show that we were able to control the pore sizes of SWNT framework membranes using different linker molecules.

The framework synthesis method can be applied not only to planar surfaces, but also to microspheres and to virtually any amine-functionalized surface, even with an irregular shape. We demonstrated this versatility with silica microspheres (diameter ~5 μm, Figure 10b). The silica microspheres were coated with PEI and then subjected to the above covalent process (8 cycles with ODA). The SWNT framework thin films were deposited on the outer surface of the microspheres, which was easily observed by the naked eye. Even silica beads with irregular shapes (for example, silica for regular column chromatography) work equally well, which opens the possibility of large scale production. It should be noted that each reaction in the covalent process for microspheres takes shorter times with gentle vortex mixing, probably due to faster mass transfer.

Hydrofluoric acid (HF) etching of the microspheres' silica cores produced hollow SWNT framework capsules, which was confirmed by TEM.[37] In addition, we demonstrated the encapsulation of gold nanoparticles inside the SWNT framework

capsules (Figure 10b bottom). First, gold nanoparticles were synthesized on the surface of silica microspheres using a slightly modified Turkevich method. Gold salts (HAuCl₄) were adsorbed on the PEI-modified silica microspheres (diameter ~5 μm), and the gold ions were reduced to gold nanoparticles by ascorbic acid in the presence of sodium citrate at room temperature. The SWNT framework thin films were deposited with ODA on these gold nanoparticle-decorated silica microspheres, and then the silica core was removed by HF etching. TEM images clearly show that gold nanoparticles (average size ~30 nm) were encapsulated in the SWNT cages, and both individual and agglomerated gold nanoparticles were observed.[37]

These new SWNT frameworks could be useful in the design and fabrication of new composite armor materials. Energetic materials or other functional nanomaterials could be introduced into the structure in analogous fashion to the covalent linkers or micro-/nanoparticles described above to tailor new functional materials to specific applications.

Publications

- Sharma R, Baik JH, Perera C, **Strano MS**: Anomalously Large Reactivity of Single Graphene Layers and Edges towards Electron Transfer Chemistries. NANO LETTERS (in press)
- Nair N, **Strano MS**: One-dimensional nanostructure-guided chain reactions: Harmonic and anharmonic interactions. PHYSICAL REVIEW B, 80 (2009) 174301.
- Song CS, Kwon T, Han JH, Shandell M, **Strano MS**: Controllable Synthesis of Single-Walled Carbon Nanotube Framework Membranes and Capsules. NANO LETTERS, 9 (2009) 4279.
- Sharma R, Nair N, **Strano MS**: Structure-Reactivity Relationships for Graphene Nanoribbons. JOURNAL OF PHYSICAL CHEMISTRY C, 113 (2009) 14771.

- Abrahamson JT, Nair N, **Strano MS**: Modeling anisotropic reaction rate increase in metal nanoparticle using carbon nanotubes as thermal conduits. NANOTECHNOLOGY, 19 (2008) 195701.

References

1. Held, M. Comparison of explosive reactive armour against different threat levels. **24**, 76-77 (1999).
2. Held, M. Effectiveness factors for explosive reactive armour systems. **24**, 70-75 (1999).
3. Trzcinski, W. A., Trebinski, R. & Cudzilo, S. Study of the reaction of model reactive armour to jet attack. **28**, 89-93 (2003).
4. Yadav, H. S., Bohra, B. M., Joshi, G. D., Sundaram, S. G. & Kamat, P. V. Study on basic mechanism of reactive armour. **45**, 207-212 (1995).
5. Held, M. Momentum theory of explosive reactive armours. **26**, 91-96 (2001).
6. Freeguard, G. F. & Marshall, D. Bullet-Resistant Glass - Review of Product and Process Technology. **11**, 25-32 (1980).
7. Abrahamson, J. T., Nair, N. & Strano, M. S. Modelling the increase in anisotropic rxn rates in metal nanoparticle oxidn using CNT. *Nanotechnology* **19**, 195701 (2008).
8. Buehler, M. J. *J. Mater. Res.* **21**, 2855 (2006).
9. Muthurajan, H., Sivabalan, R., Talawar, M. B., Anniyappan, M. & Venugopalan, S. Predixn of heat of formation and related parameters of HEM. *J. Hazard. Mater.* **A133**, 30 (2006).
10. Long, G. T., Brems, B. A. & Wight, C. A. Autocatalytic thermal decomposition kinetics of TNT. *Thermochimica Acta* **388**, 175-181 (2002).
11. Lawler, H. M., Mintmire, J. W. & White, C. T. Helical strain in CNTs. *Phys. Rev. B.* **74**, 125415 (2006).

12. Strano, M. S. et al. Electronic structure control of single-walled carbon nanotube functionalization. *Science* **301**, 1519-1522 (2003).

13. Schoutissen, H. A. J. The Diazotization of Very Weakly Basic Amines. *Journal of the American Chemical Society* **55**, 4531-4534 (1933).

14. Dyke, C. A. & Tour, J. M. Unbundled and highly functionalized carbon nanotubes from aqueous reactions. *Nano Letters* **3**, 1215-1218 (2003).

15. Brill, T. B. & James, K. J. Kinetics and Mechanisms of Thermal-Decomposition of Nitroaromatic Explosives. *Chemical Reviews* **93**, 2667-2692 (1993).

16. Cohen, R., Zeiri, Y., Wurzberg, E. & Kosloff, R. Mechanism of thermal unimolecular decomposition of TNT (2,4,6-trinitrotoluene): A DFT study. *Journal of Physical Chemistry A* **111**, 11074-11083 (2007).

17. Eesley, G. L. Generation of Nonequilibrium Electron and Lattice Temperatures in Copper by Picosecond Laser-Pulses. *Physical Review B* **33**, 2144-2151 (1986).

18. Liu, J. M., Kurz, H. & Bloembergen, N. Picosecond Time-Resolved Plasma and Temperature-Induced Changes of Reflectivity and Transmission in Silicon. *Applied Physics Letters* **41**, 643-646 (1982).

19. Paddock, C. A. & Eesley, G. L. Transient Thermoreflectance from Thin Metal-Films. *Journal of Applied Physics* **60**, 285-290 (1986).

20. Hopkins, P. E. & Norris, P. M. Thermal boundary conductance response to a change in Cr/Si interfacial properties. *Applied Physics Letters* **89**, - (2006).

21. Klopf, J. M. & Norris, P. Probing nonequilibrium dynamics with white-light femtosecond pulses. *Applied Surface Science* **253**, 6305-6309 (2007).

22. Komarov, P. L., Burzo, M. G., Kaytaz, G. & Raad, P. E. Transient thermo-reflectance measurements of the thermal conductivity and interface resistance of metallized natural and isotopically-pure silicon. *Microelectronics Journal* **34**, 1115-1118 (2003).

23. Kulish, V. V., Lage, J. L., Komarov, P. L. & Raad, P. E. A fractional-diffusion theory for calculating thermal properties of thin films from surface transient thermoreflectance measurements. *Journal of Heat Transfer-Transactions of the Asme* **123**, 1133-1138 (2001).

24. Norris, P. M. et al. Femtosecond pump-probe nondestructive examination of materials (invited). *Review of Scientific Instruments* **74**, 400-406 (2003).

25. Taketoshi, N., Baba, T. & Ono, A. Electrical delay technique in the picosecond thermoreflectance method for thermophysical property measurements of thin films. *Review of Scientific Instruments* **76**, - (2005).

26. Hopkins, P. E. & Norris, P. M. Substrate influence in electron-phonon coup ing measurements in thin Au films. *Applied Surface Science* **253**, 6289-6294 (2007).

27. Smith, A. N., Hostetler, J. L. & Norris, P. M. Thermal boundary resistance measurements using a transient thermoreflectance technique. *Microscale Thermophysical Engineering* **4**, 51-60 (2000).

28. Stevens, R. J., Smith, A. N. & Norris, P. M. Measurement of thermal boundary conductance of a series of metal-dielectric interfaces by the transient thermoreflectance technique. *Journal of Heat Transfer-Transactions of the Asme* **127**, 315-322 (2005).

29. Borca-Tasciuc, T. et al. Anisotropic thermal diffusivity of aligned multiwall carbon nanotube arrays. *Journal of Applied Physics* **98**, - (2005).

30. Ivanov, I. et al. Fast and highly anisotropic thermal transport through vertically aligned carbon nanotube arrays. *Applied Physics Letters* **89**, - (2006).

31. Shenogin, S., Bodapati, A., Xue, L., Ozisik, R. & Keblinski, P. Effect of chemical functionalization on thermal transport of carbon nanotube composites. *Applied Physics Letters* **85**, 2229-2231 (2004).

32. Kotov, N. A. (ed.) *Nanoparticle Assemblies and Superstructures* (CRC Press, Boca Raton, 2006).

33. Rao, C. N. R., Muller, A. & Cheetham, A. K. (eds.) *The Chemistry of Nanomaterials: Synthesis, Properties and Applications* (Wiley-VCH, Weinheim, 2004).

34. Nair, N., Kim, W. J., Usrey, M. L. & Strano, M. S. A structure-reactivity relationship for single walled carbon nanotubes reacting with 4-hydroxybenzene diazonium salt. *Journal of the American Chemical Society* **129**, 3946-3954 (2007).

35. Graff, R. A., Swanson, T. M. & Strano, M. S. Synthesis of nickel-nitrilotriacetic acid coupled single-walled carbon nanotubes for directed self-assembly with polyhistidine-tagged proteins. *Chemistry of Materials* **20**, 1824-1829 (2008).

36. The molecular lengths are based on the structures after AM1 semi-empirical optimization.

37. Song, C. S., Kwon, T., Han, J. H., Shandell, M. & Strano, M. S. Controllable Synthesis of Single-Walled Carbon Nanotube Framework Membranes and Capsules. *Nano Letters* **9**, 4279-4284 (2009).